

PCCP

Accepted Manuscript



This is an *Accepted Manuscript*, which has been through the Royal Society of Chemistry peer review process and has been accepted for publication.

Accepted Manuscripts are published online shortly after acceptance, before technical editing, formatting and proof reading. Using this free service, authors can make their results available to the community, in citable form, before we publish the edited article. We will replace this *Accepted Manuscript* with the edited and formatted *Advance Article* as soon as it is available.

You can find more information about *Accepted Manuscripts* in the [Information for Authors](#).

Please note that technical editing may introduce minor changes to the text and/or graphics, which may alter content. The journal's standard [Terms & Conditions](#) and the [Ethical guidelines](#) still apply. In no event shall the Royal Society of Chemistry be held responsible for any errors or omissions in this *Accepted Manuscript* or any consequences arising from the use of any information it contains.

Cite this: DOI: 10.1039/c0xx00000x

www.rsc.org/xxxxxx

ARTICLE TYPE

Changes in microstructure and physical properties of skutterudites after severe plastic deformation

Gerda Rogl,^{*a,b,d,f} Andriy Grytsiv,^{a,b,f} Jiri Bursik,^c Jelena Horky,^d Ramakrishnan Anbalagan,^e Ernst Bauer,^{b,f} Ramesh Chandra Mallik,^e Peter Rogl,^{a,f} and Michael Zehetbauer^d

Received (in XXX, XXX) Xth XXXXXXXXXX 20XX, Accepted Xth XXXXXXXXXX 20XX

DOI: 10.1039/b000000x

Abstract

The best p-type skutterudites with $ZT > 1.1$ so far are didymium (DD) filled, Fe/Co substituted, Sb-based skutterudites. $DD_{0.68}Fe_3CoSb_{12}$ was prepared using an annealing -reacting -melting - quenching technique followed by ball milling and hot pressing. After severe plastic deformation via high-pressure torsion (HPT), no phase changes but particular structural variations were achieved, leading to modified transport properties with higher ZT values. Although after measurement-induced heating some of the HPT induced defects were annealed out, a still attractive ZT -value was preserved. In this paper we focus on explanations for these changes via TEM investigations, Raman spectroscopy and texture measurements. The grain sizes and dislocation densities, evaluated from TEM images, showed that (i) the majority of cracks generated during high-pressure torsion are healed during annealing, leaving only small pores, that (ii) the grains have grown, and that (iii) the dislocation density is decreased. While Raman spectra indicate that after HPT processing and annealing the vibration modes related to the shorter Sb-Sb bonds in the Sb_4 rings are more affected than those related to the longer Sb-Sb bonds, almost no visible changes were observed in the pole intensity and/or orientation.

1. Introduction

Recently¹⁻⁶ skutterudites have been processed with high-pressure torsion (HPT) in order to plastically deform them and this way to refine the grains to nano size, to introduce defects (mainly vacancies) and enhance the dislocation density. Severe plastic deformation (SPD) means an imposition of a large plastic strain under enhanced hydrostatic pressure on a sample without changing its geometry. During this process the formation of grain boundaries occurs along several stages, typical of the stress-strain characteristics of SPD. Using the nomenclature of face centered cubic polycrystalline materials,^{7, 8} in stage II and III, numerous dislocations are generated which gradually arrange to dipoles and multi-dipoles and form cell walls (polarized dipolar cell walls, PDWs). This process causes the decrease of the crystallite size, but at that point no misorientations between the lattices on both sides of the walls are detectable yet. With further deformation during stage IV, polarized tilt walls (PTWs) develop out of the

PDWs and exhibit misorientations. This process is responsible for the grain refinement. With stage V the process comes to an end. After HPT processing the grain and crystallite sizes are smaller than before HPT and high concentrations of defects, mainly dislocations, vacancies and grain boundaries are introduced.⁹

Comparing transport properties and thermal expansion of p- or n-type skutterudites before and after HPT processing, the following features were observed: while the Seebeck coefficient is almost unchanged by severe plastic deformation, the electrical resistivity at room temperature is markedly increased after HPT. The shape of the resistivity-temperature curve (exemplarily further shown in the discussion for p-type $DD_{0.68}Fe_3CoSb_{12}$, Fig. 3a) is depending on the processing parameters (pressure, number of revolutions, processing temperature),⁶ but usually it shows metallic behavior i.e. increasing electrical resistivity, ρ , with increasing temperature. However, ρ decreases after reaching a maximum (for $DD_{0.68}Fe_3CoSb_{12}$ at about 600 K). On continuation of the measurement now with decreasing temperature this anomaly cannot be observed again. Data in further heating and cooling cycles stay within the error bar (about 3%) the same as for the first measurement with decreasing temperature indicating a stable behavior. This stable electrical resistivity is still higher than that before HPT.

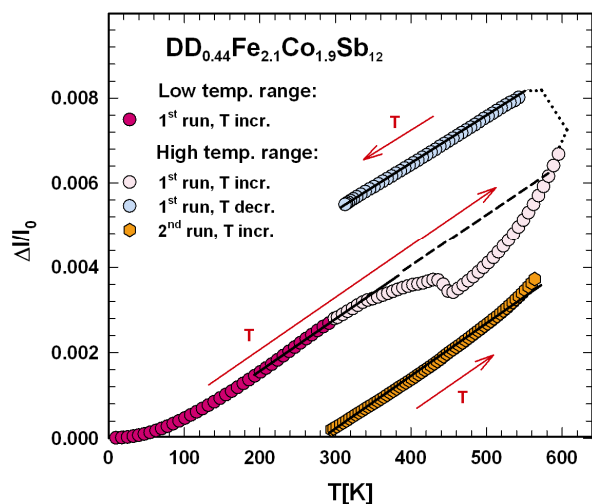
Thermal conductivity after HPT processing is slightly increasing with increasing temperature but is significantly lower than before HPT. A second measurement and/or annealing the sample at 800 K for several hours or even days increase the thermal conductivity only slightly.

Beside these above mentioned changes after HPT processing, also a slight change of the lattice parameter occurs, it is higher after HPT but annealing the sample leads to a decrease of the lattice parameter, finally flattening out to a stable value, which is still higher than the one before HPT. In parallel a change of density can be observed with a density lower after HPT but increasing after annealing, though not reaching the original high value.

All these changes and behaviors were studied by the authors in previous works¹⁻⁶ on both, p- and n-type skutterudites leading to a higher figure of merit, ZT than before HPT processing, representing an advantage for thermoelectric materials. ZT calculates as $ZT = S^2T/\rho\lambda$ with S the Seebeck coefficient, T the

absolute temperature, ρ the electrical resistivity and λ the thermal conductivity.

Studying the thermal expansion of skutterudites before and after HPT (for details see ref.5), it was found that in the low temperature range (4.2 - 300 K) the length change versus temperature results in an almost linear $\Delta l/l_0 - T$ curve increasing with increasing temperature only slightly steeper than before HPT resulting in a slightly higher coefficient of thermal expansion, α .



10

Fig. 1a. Thermal expansion $\Delta l/l_0$ versus temperature T of $DD_{0.44}Fe_{2.1}Co_{1.9}Sb_{12}$ from 4-600 K (1st run, T increasing) and from 600 K to 300 K (1st run, T decreasing) and 2nd run, from 300 K to 600 K (T increasing). Note: the last two curves are shifted for better visibility.⁵

For the high temperature range (300 - 600 K), however, a rather unexpected behavior was detected (Fig.1a). Up to about 350 K the linear increase is continued followed by a less steep slope and a kink (at about 450 K) indicating shrinking of the sample and afterwards increasing again but steeper.

20

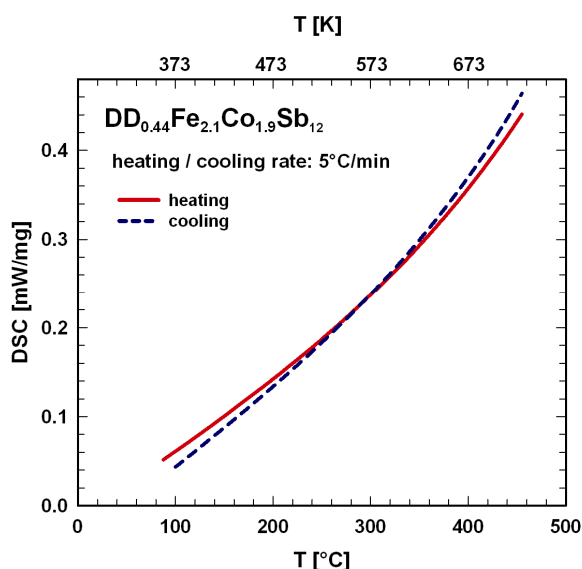


Fig. 1b. DSC curve of $DD_{0.44}Fe_{2.1}Co_{1.9}Sb_{12}$ in the temperature range of 373-753 K.⁴

25

For the measurement with decreasing temperature as well as for further measurements no kink could be detected and the slope was parallel to the one below 350 K. A second sample from the same processed disc confirmed the behavior reported above.

Here it should be noted that the DSC curve (vs. T) of the sample (for details see ref. 5) showed no anomaly in the range of 320 - 500 K (see Fig. 1b). Interestingly, the Einstein temperature, θ_E , is only about half of the value as compared to the one before HPT, whereas the Debye temperature θ_D is practically the same (θ_D and θ_E are derived from a fit according to ref. 10 to the $\Delta l/l_0 - T$ curve).⁴

Both anomalies, the maximum in the electrical resistivity curve and the shrinking of the sample were observed at higher temperatures. So far the explanation was that obviously at this certain temperature defects introduced through SPD anneal out and/or fine microcracks fuse together. In this paper we report on closer studies of these changes in the HPT processed samples, by using TEM, Raman spectroscopy and X-ray texture analyses of a $DD_{0.68}Fe_3CoSb_{12}$ skutterudite after hot pressing before (sample labeled HP) and after HPT processing (sample labeled HPT), as well as after annealing of the HPT processed sample (sample labeled HPTa).

2. Experimental

The p-type skutterudite with the nominal composition $DD_{0.70}Fe_3CoSb_{12}$ (DD stands for the natural double filler didymium from Treibacher Industrie AG, Austria, containing 4.76 mass% Pr + 95.24% Nd, and Fe, Co, Sb from Alfa Aesar, all with a purity better than 99.9 mass%) was prepared via an annealing-reaction-melting technique as described in detail in ref. 11, followed by ball milling, BM (in Ar-filled tungsten carbide vessels using a Fritsch planetary mill Pulverisette 4) and hot pressing, HP, (uniaxial HP W 200/250 2200-200-KS, Ar, 600°C, 56 MPa, 60 min).

The hot pressed cylindrical samples with a radius of 5 mm were cut into discs of a thickness of about 1 mm and were HPT-processed with a machine from W. Klement (Austria) at room temperature, or at 300°C, employing a pressure of 4 GPa during one revolution.

X-ray powder diffraction (XPD) data were collected with Gemonochromated $CuK\alpha_1$ -radiation in a HUBER-Guinier image plate recording system using 99.9999% pure Ge or Si as internal standard. X-ray spectra were used to calculate the lattice parameters (program STRUKTUR¹²), the program FULLPROF¹³ was employed for quantitative Rietveld refinements in order to determine the total filling level in combination with EDX data. The chemical composition was analyzed by electron probe microanalysis (EPMA - EDX) with an INCA Penta FETx3 - Zeiss SUPRATM55VP equipment. The crystallite size x_{cs} and the residual strain were evaluated from the XRD patterns using the MDI JADE 6.0 software (Materials Data Inc., Liverpool, CA). This method allows to calculate the crystallite size from the full width at half-maximum (FWHM) of a single diffraction peak using the formula developed by Scherrer.¹⁴ Silicon was used as internal standard to take care of instrumental broadening. The calculations of x_{cs} were performed for three well separated reflections, (240), (332) and (422) within a 2θ range from 41° to

48°. For details see ref. 15.

Raman active vibration modes were identified by Raman spectroscopy with an argon solid-state laser at $\lambda = 532$ nm (Raman and MicroPL system, HORIBA, Singapore) and an optical microscope with an MPlan N100X objective. All the data have been fitted with a Gaussian fit to get the respective peak positions.

Bulk texture measurements were carried out for three pole figures namely (013), (123), (420) by Schulz reflection methods using a Bruker D8 Discover diffractometer. The measured texture data were further analyzed by MATLAB - MTEX (free source).

A Philips CM12 STEM transmission electron microscope operated at 120 kV (TEM) and alternatively a high resolution transmission electron microscope JEOL JEM2010 FEG operated at 200 kV with point resolution of 2.3 Å (HRTEM) were used to study the details of microstructure. Both instruments are equipped with an energy dispersive X-ray (EDX) detector. Samples for TEM observations were prepared in form of thin lamellae (lateral dimensions about 10×8 μm, thickness below 100 nm) cut perpendicularly to the polished facet of material fragments using a focused ion beam (FIB) technique in a TESCAN LYRA 3 XMU FEG/SEMx/FIB scanning electron microscope.

The density of each sample was measured using Archimedes' principle in distilled water. Electrical resistivities and Seebeck coefficients were measured between 300 K and 823 K with an ULVAC-RIKO ZEM-3 system. Thermal conductivity was obtained from an ANTER Flashline 3000 unit in the temperature range of 423 K - 800 K. The measurement errors for the electrical resistivity and the Seebeck coefficient were $< 5\%$ and $< 10\%$ for the thermal conductivity.

For the measurement of the thermal expansion (length change vs. temperature) above 300 K a dynamic mechanical analyser DMA7 (Perkin Elmar Inc.) was employed (for further details see ref. 5).

3. Results and Discussion

First of all, it has to be emphasized that the XRD patterns after HPT processing of the sample $\text{DD}_{0.68}\text{Fe}_3\text{CoSb}_{12}$ (Fig 2) did not show any change of the skutterudite phase and of the filling level compared to those before HPT processing. The same observation resulted from all our previous investigations on HPT processed skutterudites regardless of p- or n-type material.¹⁻⁶ This is a clear difference to other cases where – especially in metals – significant changes in the phases' stability has been found not only because of the enhanced hydrostatic pressure but also because of the high plastic strain applied.^{16,17} Nevertheless from the X-ray diffraction patterns, shown in Fig. 2, the lattice parameter was found to increase from $a = 0.91109(1)$ nm before to $a = 0.91130(2)$ nm after HPT processing. Furthermore X-ray diffraction patterns show peak broadening after HPT processing (Fig. 2): accordingly the crystallite size decreases from $x_{\text{cs}} = 170 \pm 10$ nm to $x_{\text{cs}} = 40 \pm 5$ nm, with the internal strains increasing from $0.020 \pm 0.002\%$ to $0.152 \pm 0.004\%$. From previous investigations of the authors⁴⁻⁶ it is known that the dislocation density (before HPT being $10^{12} - 10^{13} \text{ m}^{-2}$) after HPT processing is increased by a factor of 10. This proves that HPT processing is effective for nanostructuring, but not at least due to the TEM investigations reported below; it also introduces mesoscopic defects like cracks and pores. Also the comparison of the density

before and after HPT with a change of $d_{\text{bef}} = 7.72 \text{ g cm}^{-3}$ to $d_{\text{aft HPT}} = 7.38 \text{ g cm}^{-3}$, respectively, leads to the conclusion that besides lattice defects also small microcracks are inferred by the deformation. After measurement induced heating, however, the density is higher again ($d_{\text{aft HPT ann}} = 7.56 \text{ g cm}^{-3}$).

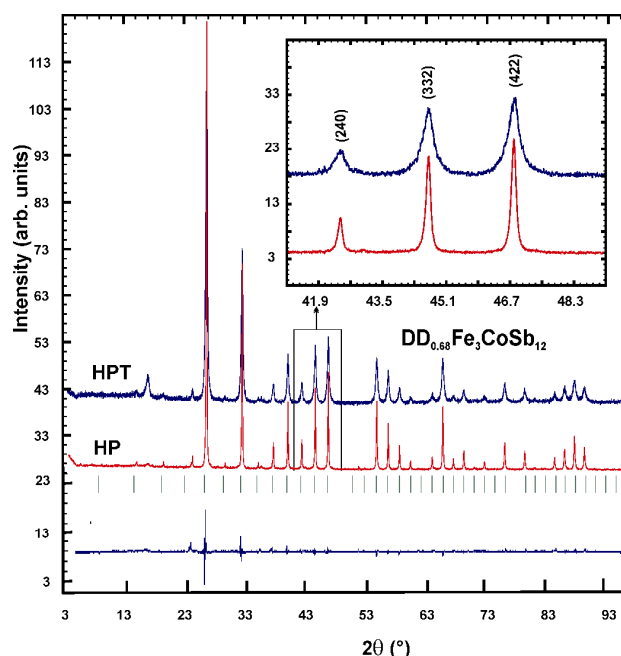


Fig. 2. X-ray diffraction pattern of $\text{DD}_{0.68}\text{Fe}_3\text{CoSb}_{12}$ before and after HPT processing. The insert documents the peak broadening as seen on the (240), (332) and (422) peaks. Note: the peak at $2\theta \approx 15^\circ$ in the spectrum for the HPT processed sample stems from the foil.

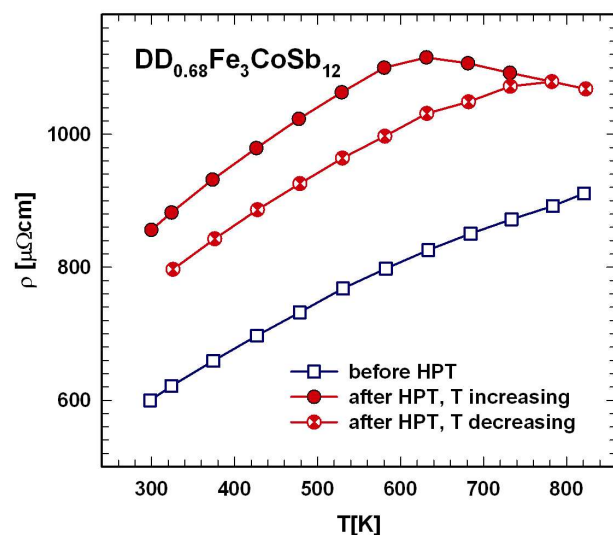


Fig. 3a. Electrical resistivity, ρ , versus temperature T of $\text{DD}_{0.68}\text{Fe}_3\text{CoSb}_{12}$ before and after HPT.

As already described in various papers of the authors,¹⁻⁶ the electrical resistivity (Fig.3a) is higher after HPT due to introduced defects, smaller grains and even small cracks, whereas the Seebeck coefficient (Fig. 3b) is not affected. During measurement induced heating it is assumed that a marked amount of the defects anneals out at higher temperature, resulting in a

decrease of the electrical resistivity. The second measurement with decreasing temperature shows still a higher resistivity but the slope is practically parallel to the one before HPT. Of course, due to the high electrical resistivity values, the power factor S^2/ρ (insert in Fig. 3d) after HPT is lower than before HPT.

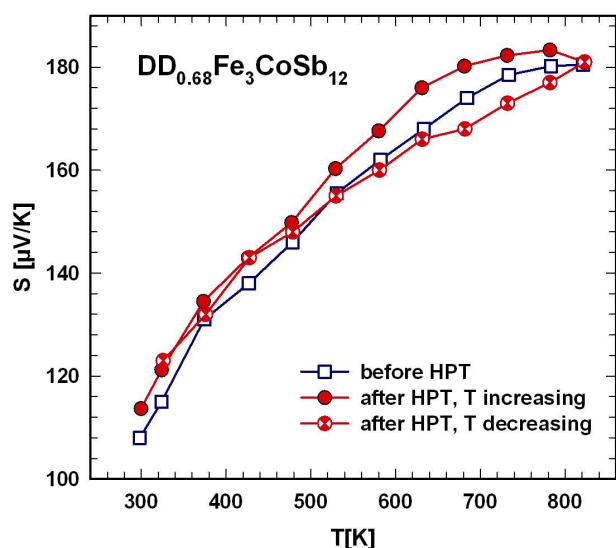


Fig. 3b. Seebeck coefficient, S , versus temperature T of $\text{DD}_{0.68}\text{Fe}_3\text{CoSb}_{12}$ before and after HPT.

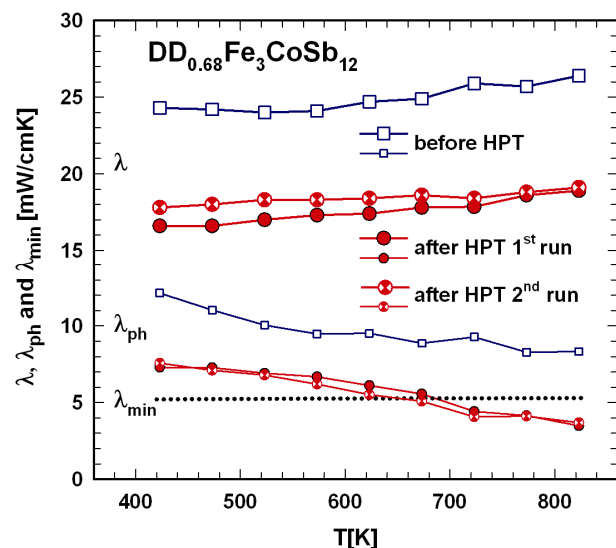


Fig. 3c. Thermal, λ , and lattice thermal conductivity, λ_{ph} , in dependence of temperature, T , of $\text{DD}_{0.68}\text{Fe}_3\text{CoSb}_{12}$ before and after HPT.

However, the decrease of the electrical conductivity is accompanied by a markedly lower thermal conductivity (Fig. 3c), i.e. it is about 50% lower than before HPT in the whole temperature range. The phonon part of the thermal conductivity λ_{ph} ($\lambda_{\text{ph}} = \lambda - \lambda_{\text{el}}$ with $\lambda_{\text{el}} = L_0 T / \rho$, where L_0 was taken as $2.0 \times 10^{-8} \text{ V}^2 \text{ K}^{-2}$, as estimated by Chaput et al.¹⁸) was calculated for $\text{DD}_{0.68}\text{Fe}_3\text{CoSb}_{12}$ before and after HPT. λ_{min} is a value derived in accordance with the theoretical concept of Cahill and Pohl,¹⁹ simulating the thermal conductivity for a glassy state of $\text{DD}_{0.68}\text{Fe}_3\text{CoSb}_{12}$. As can be seen in Fig 3c, the values of λ_{ph}

before HPT are higher than λ_{min} but after HPT they approach the range of λ_{min} even after measurement-induced annealing. The figure of merit, ZT , (Fig. 3d) is higher than before HPT resulting in $ZT > 1.3$ at 825 K, which means an increase of almost 20%.

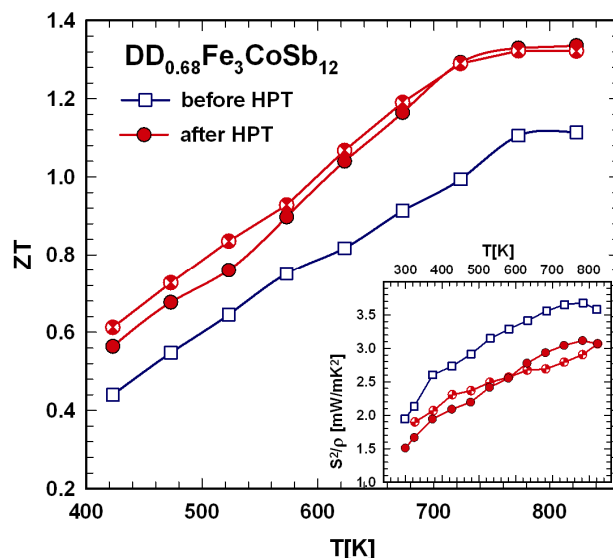


Fig. 3d. Figure of merit, ZT , in dependence of temperature, T of $\text{DD}_{0.68}\text{Fe}_3\text{CoSb}_{12}$ before and after HPT. Insert: temperature dependent power factor, S^2/ρ .

TEM observations of the sample after HPT (Figs. 4a,b) reveal small grains with an average diameter of $110 \pm 10 \text{ nm}$ showing a rather homogeneous size distribution. Long intergranular cracks, already visible in STEM during the lamella preparation could be observed (Fig 4a). The dislocation density in the HPT sample was around $8 \times 10^{13} \text{ m}^{-2}$. Annealing of the HPT sample in the range 300–850 K resulted in larger equiaxed grains with an average diameter of $320 \pm 50 \text{ nm}$ (Figs. 5a,b) as evaluated by the linear intercept method. There are dislocation walls and a lower dislocation density inside of the grains of the order of $1 \times 10^{13} \text{ m}^{-2}$. These values compare well with those derived from TEM investigations of n-type $\text{Sr}_{0.07}\text{Ba}_{0.07}\text{Yb}_{0.07}\text{Co}_4\text{Sb}_{12}$.¹³ There is a commonly known discrepancy between grain size and/or crystallite size, as well as dislocation densities gained from XRD patterns and obtained with the linear intercept method (using TEM or SEM images) with higher values for the latter method. The reasons for this discrepancy were explained in detail in ref. 3. Cracks obviously are almost annealed out after measurement-induced heating and only few of them were found near the sample surface. Pores (Fig. 5b) were occasionally observed at grain boundaries and are obviously remnants of cracks, now almost annealed out. It is important to note that neither oxidation nor secondary phases were observed.

These observations confirm that after these structural changes due to HPT processing not only the electrical resistivity and in parallel the thermal conductivity but also the thermal expansion is affected. The cracks, small grains and increased density of defects explain the elevated electrical resistivity, which linearly increases with increasing temperature (temperature effect only); see Figs 3a and 6a,b. In parallel, however, some fusion of cracks takes place, the grains grow, vacancies and dislocations become less, and thus, with further on increasing temperature, the electrical resistivity decreases. The structural effect is stronger than the influence of the temperature as can also be seen in Figs. 6a,b.

When the temperature decreases, as expected, the electrical resistivity decreases with decreasing temperature (temperature effect). Additional measurement runs, with increasing and decreasing temperature, now show the same identical ρ -T curves without any anomalies (see also refs. 3,5,6).

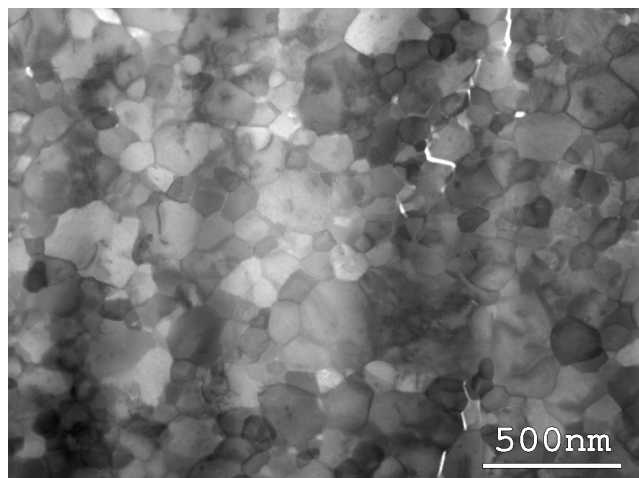


Fig. 4a. STEM micrograph of $DD_{0.68}Fe_3CoSb_{12}$ after HPT processing.

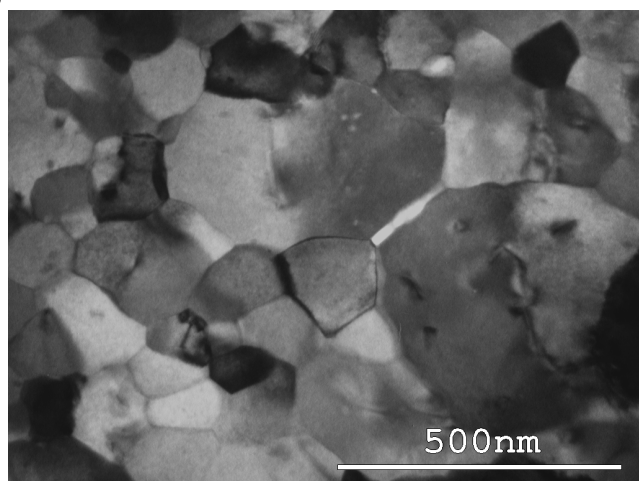


Fig. 4b. STEM micrograph of $DD_{0.68}Fe_3CoSb_{12}$ after HPT processing (higher magnification).

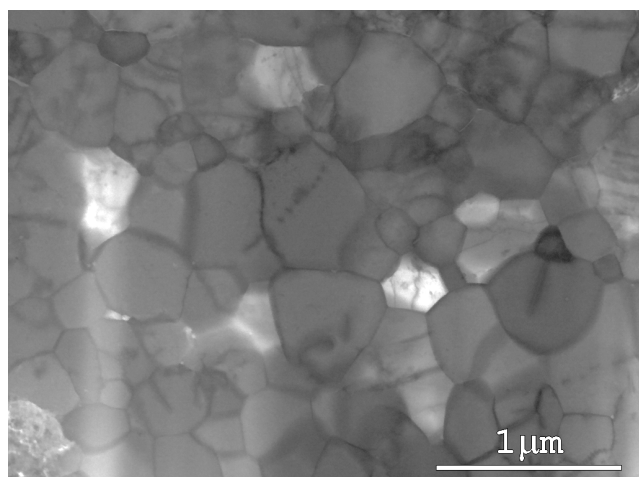


Fig. 5a. STEM micrograph of $DD_{0.68}Fe_3CoSb_{12}$ after HPT

processing, after measurement induced annealing.

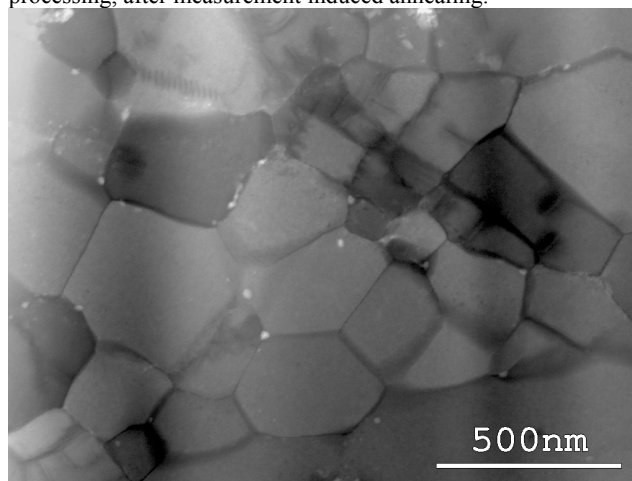


Fig. 5b. STEM micrograph of $DD_{0.68}Fe_3CoSb_{12}$ after HPT processing, after measurement-induced annealing (higher magnification).

The structural changes as observed by TEM not only affect the electrical resistivity but also the thermal expansion of the sample. As displayed in Figs. 1a and 6a,b, at a certain temperature the sample shrinks with increasing temperature, an effect of grain growing and in parallel of the fusion of the cracks. As soon as there are only small pores left (minimum in the $\Delta l/l_0$ - T curve), the sample expands with increasing temperature. As can be seen in Fig. 6a, sample $DD_{0.68}Fe_3CoSb_{12}$ shows a minimum in the $\Delta l/l_0$ - T curve at about 550 K. At about the same temperature also the ρ -T curve starts to bend. For $Sr_{0.07}Ba_{0.07}Yb_{0.07}Co_4Sb_{12}$ the minimum of the $\Delta l/l_0$ - T curve appears at the same temperature at which the electrical resistivity exhibits a maximum (Fig. 6b). As can be seen in Fig. 1a, afterwards the length change is directly proportional to the temperature. The minimum for the sample measured in and perpendicular to the press direction occurs not exactly at the same temperature. The reason might be that there is a difference in the crystal structure in relation to the torsion axis, which might influence the annealing out of vacancies as recently observed for Cu and Ni.²⁰ So far this is a speculation and further experiments will be necessary for confirmation.

A positive effect occurs for the thermal conductivity, λ : due to smaller grains, a higher dislocation density, defects and cracks, the thermal conductivity is lower than before HPT processing; especially the phonon part, λ_{ph} is in the range of the minimum thermal conductivity.

The micro-structural change during heating of the sample fortunately has almost no impact on the thermal conductivity. As a net effect, the figure of merit of the HPT processed sample is 20% higher even after measurement-induced annealing.

The TEM investigations confirmed that after annealing the cracks may have disappeared but that there are pores and some of the deformation induced defects e.g. dislocations are left. This means that the SPD beneficiary effect is not completely gone and that the “thermally stable” sample still has a higher ZT value than before SPD.

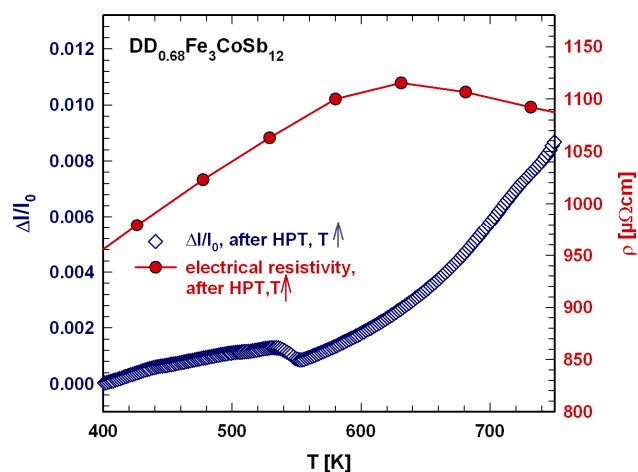


Fig. 6a. Thermal expansion, $\Delta l/l_0$, versus temperature T as well as temperature dependent electrical resistivity, ρ , of HPT processed p-type $\text{DD}_{0.68}\text{Fe}_3\text{CoSb}_{12}$.

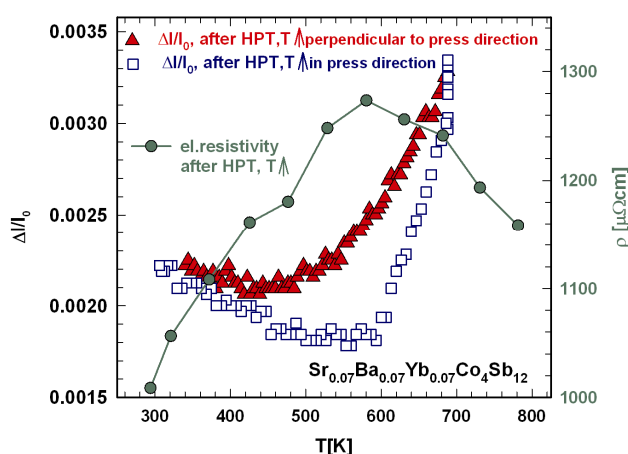


Fig. 6b. Thermal expansion, $\Delta l/l_0$, versus temperature T measured perpendicular to and in press direction as well as temperature dependent electrical resistivity, ρ , of HPT processed n-type $\text{Sr}_{0.07}\text{Ba}_{0.07}\text{Yb}_{0.07}\text{Co}_4\text{Sb}_{12}$.

was found by the authors²⁷ for other $\text{DD}_y(\text{Fe}_{1-x}\text{Co}_x)_4\text{Sb}_{12}$ skutterudites. The spectrum for the HPT sample shows an additional softening of the F_g , A_g and E_g modes in the high-energy region as well as peak broadening. These two modifications of the spectrum indicate that the vibration modes related to the shorter Sb-Sb bonds in the Sb_4 rings are more affected than those with the longer Sb-Sb bond. After annealing, because of an increase of the grain size, no broadening of the peaks can be observed any more; as a matter of fact, the spectrum of HPTa is quite undistinguishable from the sample HP, before HPT processing.

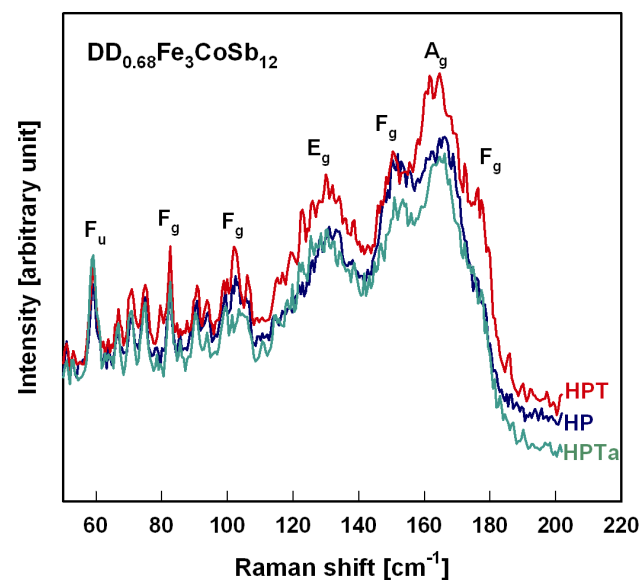


Fig. 7. Raman shift of $\text{DD}_{0.68}\text{Fe}_3\text{CoSb}_{12}$ after hot pressing, before HPT (HP), after HPT (HPT) and after annealing the HPT sample (HPTa).

Texture measurements were performed on all three samples HP, HPT and HPTa, on the plane perpendicular to the HPT pressing direction. No distinguishable changes in the pole intensity and/or orientation could be found. It has been repeatedly observed in HPT processing of metals that the HPT induced textures are the less significant the smaller the grain size becomes; the explanation for that is that below a certain grain size (in metals around 20 nm) grain boundary sliding starts at the cost of grain interior deformation governed by dislocations.^{28,29}

4. Conclusions

In this work TEM investigations were undertaken which helped to clarify some unsolved phenomena occurring after SPD of p- and n-type skutterudites. It could be shown that the HPT-processed sample ($\text{DD}_{0.68}\text{Fe}_3\text{CoSb}_{12}$) does not show any new or secondary phases and/or impurities, but microcracks and pores, an enhanced number of dislocations and smaller grains. Furthermore it was made evident from TEM images that after measurement-induced heating the grains had grown, the major part of cracks was fused to pores and that the dislocation density was smaller than immediately after SPD processing. These effects explain the behavior of the electrical resistivity, first increasing with increasing temperature but then decreasing even

in absolute terms, due to increased annealing of the defects mentioned above. Although the electrical resistivity even after annealing the HPT sample is higher than originally, the lower thermal conductivity still overcompensates this disadvantage resulting as net effect in about 20% higher ZT values, with ZT>1.3. The same structure change during heating the HPT processed sample has an impact on the length change of the sample, explaining the minimum in the expansion vs. T curve. The stretching of the Sb₄ ring in the shorter direction was disturbed more than in the long direction. No visible changes in the pole intensity, thus in the orientation distribution of crystallites could be detected.

Notes

^a Institute of Physical Chemistry, University of Vienna, Währingerstrasse 42, A-1090 Wien, Austria, Fax: +43142779524, Tel: +431427752451, gerda.rogl@univie.ac.at, peter.franz.rogl@univie.ac.at.

^b Institute of Solid State Physics, Vienna University of Technology, Wiedner Hauptstrasse 8-10, A-1040 Wien, Austria, Tel: +4315880113160, andriy.grytsiv@univie.ac.at, bauer@ipf.tuwien.ac.at

^c Institute of Physics of Materials, Academy of Sciences of the Czech Republic, Žitkova 22, 61662 Brno, Czech Republic, Tel: +532290473, bursik@ipm.cz

^d Research Group Physics of Nanostructured Materials, University of Vienna, Boltzmanngasse 5, A-1090 Wien, Austria, Tel: +431427772843 jelena.horky@univie.ac.at, michael.zehetbauer@univie.ac.at,

^e Thermoelectric Materials and Devices Laboratory, Department of Physics, Indian Institute of Science, Bangalore 560 012, India, Tel: +918022932450, anbusrr@gmail.com, rameshmallik@gmail.com

^f Christian Doppler Laboratory for Thermoelectricity, Währingerstrasse 42, A-1090 Wien, Austria and Wiedner Hauptstrasse 8-10, A-1040 Wien, Austria, Fax: +43142779524, Tel: +431427752451

Acknowledgements

The authors thank the “Christian Doppler Laboratory for Thermoelectricity”, Vienna Austria, the Institutional Project RVO: 68081723 and the OEAD project CZ12/13 for support of this research. We thank Prof. S. Suwas at the Department of Material Engineering (Institute of Science, Bangalore, India) for the texture measurement.

References

- G. Rogl, M. Zehetbauer, M. Kerber, P. Rogl and E. Bauer, *Mater. Sci. Forum*, 2011, **667-669**, 1089-1094.
- G. Rogl, D. Setman, E. Schafner, J. Horky, M. Kerber, M. Zehetbauer, M. Falmbigl, P. Rogl, E. Royanian and E. Bauer, *Acta Materialia*, 2012, **60**, 2146-2157.
- G. Rogl, Z. Aabdin, E. Schafner, J. Horky, D. Setman, M. Zehetbauer, M. Kriegisch, O. Eibl, A. Grytsiv, E. Bauer, M. Reinecker, W. Schranz and P. Rogl, *J. Alloys Compd.*, **537**, 183-189, 2012.
- G. Rogl, D. Setman, E. Schafner, J. Horky, M. Kerber¹, M. Zehetbauer, M. Falmbigl, P. Rogl and E. Bauer, *New Materials for Thermoelectric Applications: Theory and Experiment*, NATO Science for Peace and Security Series B: Physics and Biophysics, V. Zlatic and A. Hewson (eds.), Springer Science+Business Media Dordrecht, NL, chapt. 7, pps. 80-91, 2013.
- G. Rogl, P. Rogl, E. Bauer and M. Zehetbauer, *Thermoelectric Nanomaterials*, Kunihito Kuomoto and Takao Mori (eds.), Springer Series in Materials Science, **182**, 193-254, 2013.
- G. Rogl, A. Grytsiv, P. Rogl, E. Royanian, E. Bauer, J. Horky, D. Setman, E. Schafner and M. Zehetbauer, *Acta Materialia*, **61**, 6778-6788, 2013.
- M. Zehetbauer and V. Seumer, *Acta Metall. Mater.*, **41** (2), 577 and 589, 1993.
- E. Schafner, K. Simon, S. Bernstorff, G. Tichy, T. Ungar and M. J. Zehetbauer, *Acta mater.*, **53**, 315, 2005.
- M. Zehetbauer, H. P. Stüwe, A. Vorhauer, E. Schafner and J. Kohut, *Adv. Eng. Mater.*, **5**, 330-337, 2003.
- G. D. Mukherjee, C. Bansal and A. Chatterjee, *Phys. Rev. Lett.*, **76**(11), 1876, 1996.
- G. Rogl, A. Grytsiv, P. Rogl, E. Bauer and M. Zehetbauer, *Solid State Phenomena*, **170**, 240-243, 2011.
- W. Wacha, *Diploma thesis*, University of Technology, Vienna, Austria, 1989.
- J. Rodríguez-Carvajal, Satellite Meeting on Powder Diffraction of the XV Int. Union of Crystallography Congress, Talence, France, 127, 1990.
- P. Scherrer, *Nachrichten der Gesellschaft der Wissenschaften zu Göttingen*, **2**, 98, 1918.
- L. Zhang, A. Grytsiv, M. Kerber, P. Rogl, E. Bauer, M. J. Zehetbauer, J. Wosik and G. E. Nauer, *J. Alloys Compd.*, **481**, 106-115, 2009.
- B.B. Straumal, A.A. Mazilkin, B. Baretzky, G. Schütz, E. Rabkin, R.Z. Valiev, *Mater. Trans.*, **53**, 63-71, 2012.
- B.B. Straumal, A.S. Gornakova, A.A. Mazilkin, O.B. Fabrichnaya, M.J. Kriegel, B. Baretzky, J.-Z. Jiang, S.V. Dobatkin, *Mater. Lett.* **81**, 225–228, 2012.
- L. Chaput, P. Pecher, J. Tobola and H. Scherrer, *Phys. Rev. B*, **72**, 085126, 2005.
- D. Cahill and R. Pohl, *Solid State Commun.*, **70**, 927, 1989.
- B. Oberdorfer, D. Setman, E. M. Steyskal, A. Hohenwarther, W. Sprengel, M. Zehetbauer, R. Pippa and R. Würschum, *Acta Mater.*, **68**, 189-195, 2014.
- R. Venkatasubramanian, E. Sivola, T. Colpitts and B. O’Quinn, *Nature*, **413**, 597, 2001.
- M. Rotter, P. Rogl, A. Grytsiv, W. Wolf, M. Kirsch, A. Mirone, *Phys. Rev. B*, **77**, 144301, 2008.
- P. Lu, Z. Shen and X. Hu, *Physica B Phys. Cond. Matter*, **405**(11), 2589, 2010.
- J. Penga, X. Liu, J. He and J. Yang, *Proc. Eng.*, **1877**, 121-127, 2012.
- R. H. Liu, J. Yang, X. H. Chen, X. Shi, L. D. Chen and C. Uher, *Intermetallics*, **19**, 1747–1751, 2011.
- L. X. Li, H. Liu, J. Y. Wang, X. B. Hu, S. R. Zhao, H. D. Jiang, Q. J. Huang, H. H. Wang and Z. F. Li, *Chem. Phys. Lett.*, **347**, 373-377, 2001.
- G. Rogl, A. Grytsiv, P. Rogl, E. Bauer, M. Hochenhofer, R. Anbalagan, R.C. Mallik and E. Schafner, *Acta Mater.*, **76**, 434-448, 2014.
- Y. Ivanisenko, W. Skrotzki, R. Chulist, T. Lippmann and L. Kurmanaeva, *Ser. Mater.*, **66**, 131-134, 2012.
- W. Skrotzki, A. Eschke, B. Jóni, T. Ungár, L.S. Tóth, Yu. Ivanisenko and L. Kurmanaeva, *Acta Mater.*, **61**, 7271-7284, 2013.